Theory of the ripple phase in hydrated phospholipid bilayers

J. M. Carlson and J. P. Sethna
Laboratory of Atomic and Solid State Physics, Cornell University, Ithaca, New York 14853-2501
(Received 24 April 1987)

We begin with a one-dimensional discrete microscopic model for the ripple phase which is based on the packing competition between molecular head groups and hydrocarbon chains in the bilayer. This model leads to three distinct phases: (1) uniformly tilted chains, as in the low-temperature phase $L_{\beta'}$; (2) uniform chain spacing with zero tilt, which we associate with the high-temperature phase L_α; (3) long-wavelength periodic density modulation like the $P_{\beta'}$ phase. The minimum-energy configuration in the modulated regime is composed of pinched regions of closely spaced chains separated by gaps. In the continuum limit, the bulk free energy of the pinched regions is described by a frustrated ϕ^4 theory, and the gaps give rise to a defect term. The frustration may be thought of in two ways. It produces spontaneous splay of the hydrocarbon chains in the bulk, and it makes a negative contribution to the energy associated with the defect. Viewing the frustration the second way, we find that the modulated phase is preferred when the total energy of the defect becomes sufficiently negative.

I. INTRODUCTION

The smectic ripple phase $P_{\beta'}$ is observed in hydrated lipid bilayers between the low-temperature gel phase $L_{\beta'}$, and the high-temperature liquid phase L_α.[1,2] These three bilayer phases are illustrated schematically in Fig. 1. Molecules which form the ripple phase, for example phosphatidylcholine (PC), consist of a hydrophilic polar head group joined by a glycerol backbone to a pair of hydrophobic hydrocarbon chains.[3] For wide ranges of temperature and water concentration the amphiphilic nature of these molecules causes them to form bilayers. In the high-temperature smectic-A phase L_α the chains are flexible, and there is liquidlike ordering of the molecules within each bilayer, while in the low-temperature smectic-G phase $L_{\beta'}$ the hydrocarbon chains are rigid and tilted with respect to the bilayer normal. In the intermediate phase $P_{\beta'}$, the layers are corrugated with respect to an axis parallel to the mean bilayer plane, so that a cross section of the bilayer along that axis forms a sawtoothlike pattern.[1,4] Experimentally, both freeze fracture and x-ray diffraction measurements show this phase is characterized by two-dimensional long-wavelength asymmetric ripples (i.e., one side of the sawtoothlike corrugation is longer than the other side) with a periodicity of approximately 120–160 Å, corresponding to 12–20 molecules.[5,6] The first-order transition to L_α, referred to as the main transition, is well understood in terms of melting of some of the degrees of freedom within the hydrocarbon chains.[7] However, the first-order transition to $P_{\beta'}$, often called the pretransition, which occurs at temperatures slightly below the main transition, is much less well understood.

Current models for the ripple phase fall into three main categories: (1) macroscopic theories, in which the bilayer is treated as a continuous membrane, and its elastic properties (e.g., bilayer or monolayer curvature energy) are considered; (2) microscopic theories, which are based on the packing properties of individual molecules (e.g., the head group chain packing size competition); (3) completely different approaches (e.g., the interaction between layers). A discussion of previous theoretical work appears in Appendix A. What distinguishes our work from other models is that in our model the minimum-

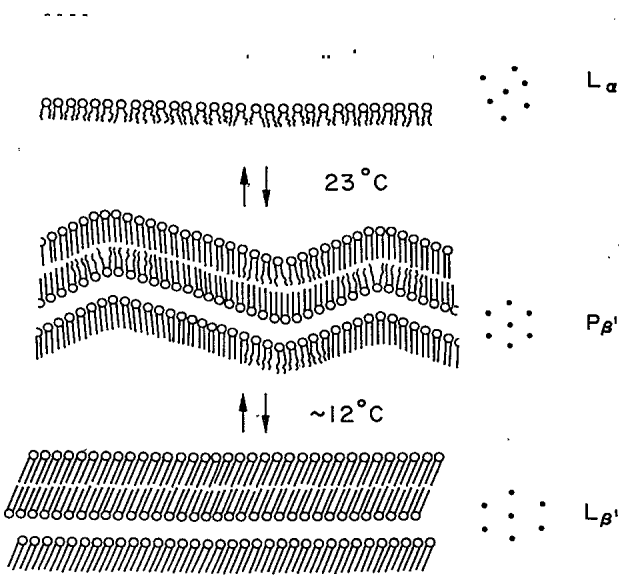

FIG. 1. Thermotropic phases of dimyristoylphosphatidycholine (DMPC) in excess water. In the high-temperature phase L_α, the chains are melted, and there is liquidlike ordering within the layer. In the low-temperature phase $L_{\beta'}$ the chains are rigid and tilted with respect to the bilayer normal. The intermediate $P_{\beta'}$ phase is characterized by long-wavelength asymmetric rippling of the bilayers. Inset at right shows intermolecular ordering within a layer [due to Janiak, Small, and Shipley (Ref. 18)].

energy configuration in the modulating regime can be described in terms of a regular array of defects, which are places where the molecular orientation shifts abruptly. These defects may be responsible for the relatively sharp peaks of the sawtooth pattern which is observed in freeze fracture experiments.[4] As we will show, the defects are a natural result of the packing competition between head groups and chains. An expression for the free-energy density which is based on the packing competition gives rise to a modulation in the chain density in one regime. Our model describes the limit in which the low-density regions (the defects) shrink to the size of the intermolecular spacing.

We begin with a discrete microscopic model for the ripple phase, which is inspired by de Gennes's for *pincements de Skoullious,* a modulating phase which was thought to appear in columnar arrangements of certain discotic molecules.[8] De Gennes's model exploits the inherent competition which arises when molecules which have two incommensurate length scales are packed together, to show that in one regime the column decomposes into a periodic sequence of pinched regions. Packing competition is also present in PC bilayers because the effective head group area is greater than the total cross-sectional area of the hydrocarbon chain pair.

In our model each lipid molecule is represented by a head group attached to a single chain, which represents the center of mass of the chain pair. The local packing properties of a one-dimensional monolayer are described in terms of pair interactions between nearest neighbors. The separation h between adjacent head groups exceeds the minimum-energy chain separation r_0. This competition leads to three distinct phases: (1) uniform tilt of the chains with respect to the normal to the head group layer, as in the gel phase $L_{\beta'}$; (2) uniform spacing with zero tilt, similar to the high-temperature phase L_α; (3) long-wavelength periodic density modulation like the $P_{\beta'}$ phase. The minimum-energy configuration depends on the size mismatch h/r_0 and the strengths of the pair interactions. In this paper we will compare the phase diagram predicted by the model with a typical experimental phase diagram. In both cases the modulation wavelength is typically about 15 molecules per period, the wavelength increases linearly with increased hydrocarbon chain length,[5] and the transition from uniform tilt to modulation is first order.

The theoretical modulated phase is composed of periodic sequences of closely packed chains, separated by large gaps in the chain spacing, similar to the structure found by Godrèche and de Seze for de Gennes's model.[9] Clearly the most striking experimental feature of the $P_{\beta'}$ phase is the fact that the layers bend out of the mean bilayer plane in an asymmetric sawtooth pattern. However, because we constrain the head group layer to be rigid and flat in our model and for simplicity assume that the molecules are symmetric, the predicted modulation is a symmetric one-dimensional density modulation of the hydrocarbon chains. To draw a more direct connection between the theoretical and experimental modulated phases, we must consider what might happen if we were to include additional degrees of freedom as small perturbations to our model. Figure 2(a) is the predicted one-dimensional symmetric modulated phase for our model. In Fig. 2(b) we show how the modulation becomes asymmetric when the asymmetry of the molecules is included in our calculations. Figure 2(c) illustrates that if we also include melting in our model, a few of the chains near the gaps should melt because of the extra available space. Finally, in Fig. 2(d) we illustrate the asymmetric two-dimensional modulation we believe should result if we were to include the second half of the bilayer, and allow the layers to bend. To minimize the empty space between the monolayers, we speculate that the melted (and hence thinnest) region of the upper monolayer would roughly coincide with the region where the chains are fully extended with zero tilt (the thickest region) in the lower monolayer. When these bilayers are allowed to bend, the peak of the corrugation should occur where the upper layer is rigid (to bring the hydrocarbon chains closer together thus gaining van der Waals energy) and the lower layer is melted (because it does not cost much energy to pull the melted chains somewhat farther apart).

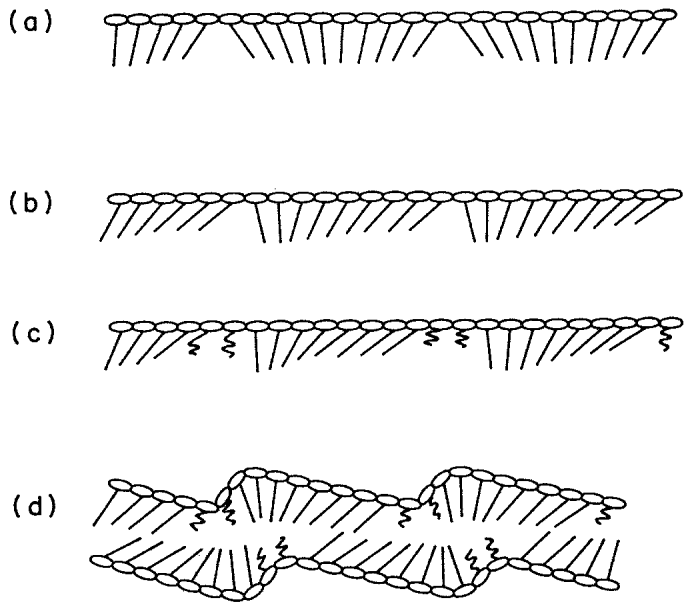

FIG. 2. The predicted modulated phase and possible results of adding some of the neglected degrees of freedom as perturbations to the model. (a) The minimum-energy configuration in the modulated phase is composed of pinched regions of closely spaced chains separated by gaps in the chain spacing. (b) When the asymmetry of the molecule ($\phi_0 \neq 0$) is included the modulation becomes asymmetric. (c) We expect that when chain melting is included a few of the chains near the gaps will melt because of the extra available space. (d) When the second half of the bilayer is included and the layer is allowed to bend, we expect that the two monolayers will line up in a way that will minimize the empty space between them, and that the peaks in the corrugation will occur where the chains in the upper layer are fully extended (so that bending brings the chains closer together thus gaining energy), and the chains in the lower layer are melted (in which case increasing their separation somewhat costs only a small amount of energy).

We have studied the long-wavelength limit of our model, and find that the most important features of the free energy in the high-density regions can be described by a frustrated ϕ^4 theory (i.e., a ϕ^4 theory where the minimum-energy gradient is nonzero), while the core energy associated with the gaps contributes a defect term. Analytical results are obtained near the critical lines in the continuum model. In the modulated phase, near the phase boundary with the tilted phase, we find that the minimum-energy configuration approaches a solitonlike structure, in which the antisoliton counterparts are the gaps.

In the continuum model, the frustration is associated with a negative total divergence term (a term proportional to the gradient of the order parameter) in the free energy, and it may be thought of in two ways. First, it produces a spontaneous inward splay of the hydrocarbon chains in the bulk. Second, it can be integrated exactly and makes a negative contribution to the energy at the gap. Viewing the frustration the second way, we find that the modulated phase is preferred when the energy of the gap becomes sufficiently negative.

Other frustrated liquid-crystal systems have similar descriptions in terms of free energies with defect terms and total divergences. Two examples are the blue phases, which are observed in cholesteric fluids,[10] and the boojums, which are observed in tilted chiral smectic films.[11] These systems also have exotic modulated phases which are composed of regions in which the molecules are arranged in local low-energy configurations (like the high-density region of the theoretical ripple phase), separated by defects (like the gaps). These systems are frustrated because the local low-energy configuration cannot fill space. We believe that there are many other systems for which a similar description would apply. The ripple phase provides a particularly compelling example because the analysis is so straightforward.

II. DISCRETE MODEL

We propose a one-dimensional model which in one regime produces a modulation in the hydrocarbon chain positions. The model is based on what we believe are the essential features responsible for the ripple phase in lipid bilayers: the van der Waals attraction between hydrocarbon chains, and the packing competition between head groups and chains. The following experimental results support our choice. First, the $P_{\beta'}$ phase has not been observed in phosphatidylethanolamine (PE) which differs from PC only in its slightly smaller head group size.[12] Second, the pretransition temperature, like the main transition temperature, increases as the hydrocarbon chain length is increased, which suggests that the attraction between chains is important.[7] While the proximity of the chain melting transition suggests that melting may play a role in the pretransition, we will not explicitly include melting in this model. Melting is an important feature for certain aspects of the problem. For example, nuclear resonance experiments and diffusion measurements indicate that both fluid and solid regions exist in the $P_{\beta'}$ phase.[13] In addition, the latent heat of the pretransition is roughly one-tenth the size of the latent heat of the main transition,[7] suggesting that a few of the chains may be melted in the $P_{\beta'}$ phase. However, we believe that the packing competition, rather than melting, is the driving force behind the modulated structure. A possible extension of our model which includes melting should explain the nuclear resonance and diffusion data, indicate why all of the phase transitions are first order experimentally, and give estimates for the relative size of the latent heats.

Other molecular features which we have not explicitly accounted for are the second hydrocarbon chain and the interaction between adjacent head groups. However, these merely alter the effective interaction between chain-pair centers. For simplicity we have ignored interlayer interactions, thermal fluctuations, anharmonic interactions between head groups and chains, and the preferred chain tilt angle ϕ_0. Strictly speaking, the asymmetry of the molecule suggests that ϕ_0 is different from zero. Keeping $\phi_0 \neq 0$ should break the symmetry of the modulation, and make the transitions first order (although we believe the transitions are first order because of chain melting, rather than the asymmetry of the molecule). Finally, we assume that the observed layer shape distortion, or rippling, in the $P_{\beta'}$ phase is a result of the chain density modulation rather than a driving force for the transition. This assumption cannot be made for the micellar and hexagonal phases, where the curvature is much larger.[14] Figure 2 illustrates how we believe our predicted modulated phase should change were we to include some of these additional degrees of freedom in our model.

A short segment of a monolayer of the system is illustrated schematically in Fig. 3. The distance h between adjacent head groups represents the effective head group size, and the head group layer is rigid and flat. The single chain associated with each head group represents the average position of the chain pair.

As illustrated in Fig. 3, the nth chain makes an angle θ_n with respect to the normal to the head group layer. We say θ_n is positive when the chain tilts to the left of the bilayer normal. The distance between adjacent

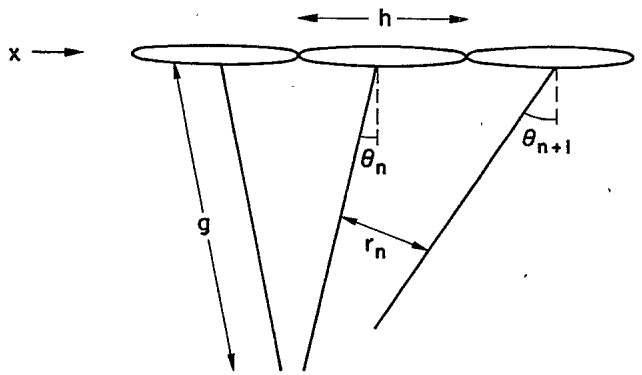

FIG. 3. A short segment of a monolayer of the model system. The head groups are fixed a distance h apart, and the chains have length g. The nth chain makes an angle θ_n with respect to the normal to the head group layer. The average separation of the nth and $(n+1)$th chains is r_n. Note that the chains can get closer by tilting.

chains is given by the length of the median of the tallest isosceles trapezoid that can be drawn between them,

$$r_n = h\cos\left[\frac{\theta_{n+1}+\theta_n}{2}\right] - g\sin\left[\frac{\theta_{n+1}-\theta_n}{2}\right], \quad (1)$$

where g is the hydrocarbon chain length. We chose this elaborate form for r_n to describe the chain separation to ensure that it had the important symmetries of the model. For parallel chains $\theta_{n+1}=\theta_n$, and $r_n = h\cos\theta_n$ is the perpendicular distance between the chains.

The free energy is a functional of the scalar order parameter θ_n, which describes the state of the system. It is a *coarse-grained* free energy because each molecule is described in terms of a single degree of freedom, which in this case is the local tilt of the chains with respect to the head group layer. In this picture, we imagine that we have integrated over all other molecular degrees of freedom, so that only θ_n remains. The other degrees of freedom give rise to phenomenological parameters, like head size and chain length, which represent the average quantities over true molecular configurations. Once this is done, the free energy of the system is given in terms of two pair interactions.[15] The first, $U(r)$, describes the van der Waals interaction between adjacent chains, and is illustrated in Fig. 4(a). $U(r)$ has a minimum at $r=r_0$, with $r_0 < h$ (competition plays a role in the free energy through this size mismatch). The strength G of $U(r)$ is linearly proportional to the length g of the hydrocarbon chains.[16] The important nonlinearities in this problem are contained in $U(r)$, which may be particularly soft due to the proximity of the chain melting transition. The second contribution comes from the coupling between head groups and chains. For the nth molecule this will be a function of θ_n alone: $E_n = F(\theta_n)$. Because we have already accounted for the important nonlinearities in $U(r)$, we will assume this is given by a simple harmonic interaction, which we write in the form

$$E_n = \tfrac{1}{2}W\sin^2(\theta_n - \phi_0) . \quad (2)$$

For simplicity we set $\phi_0=0$, in which case the free-energy density is given by

$$f = \frac{1}{N}\sum_{n=1}^{N} U(r_n) + \tfrac{1}{2}W\sin^2\theta_n . \quad (3)$$

The next step is to look for the structures which minimize f.

III. TYPES OF ORDER

A. Uniform solutions

Uniform solutions are characterized by constant tilt of the chains with respect to the head group layer $\theta=\bar{\theta}$ ($\bar{r}=h\cos\bar{\theta}$), and the constant free energy density is

$$f(\bar{\theta}) = U(\bar{r}) + \tfrac{1}{2}W\sin^2\bar{\theta} . \quad (4)$$

As illustrated in Fig. 5(a), $f(\bar{\theta})$ is an even function of $\bar{\theta}$

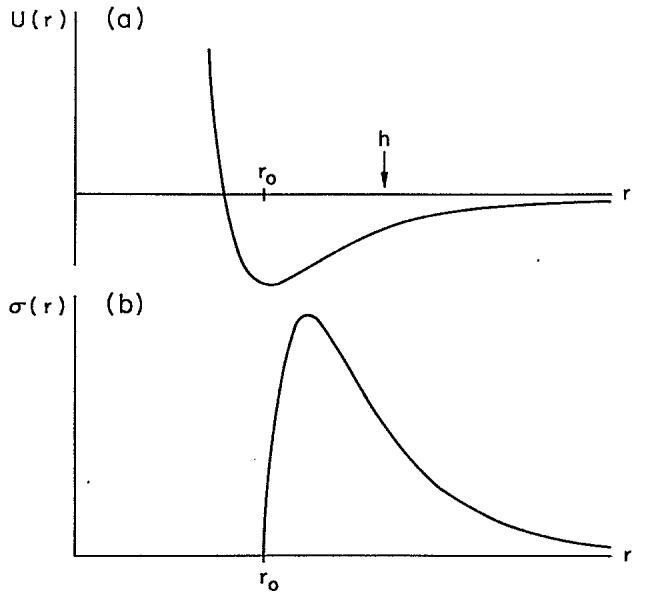

FIG. 4. The interaction between adjacent chains. (a) The potential $U(r)$ represents the van der Waals energy of neighboring chains. For this model, the most important feature of $U(r)$ is that it is soft. (b) The force between adjacent chains, $\sigma(r)=dU(r)/dr$.

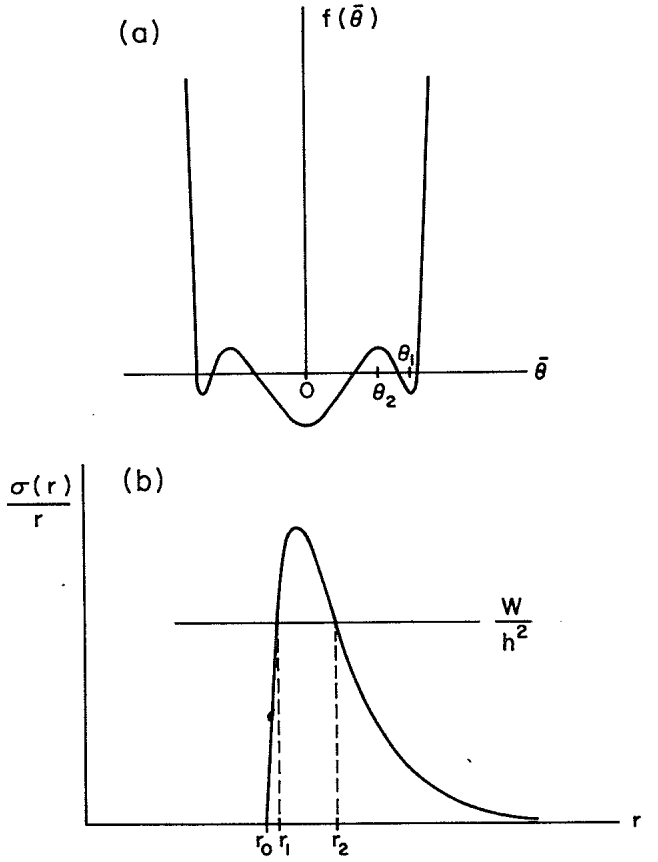

FIG. 5. Uniform solutions. (a) For certain ranges of the parameters, the free energy of a uniform solution, $f(\bar{\theta})$, will have three local minima, two corresponding to the $\pm\theta_1$ tilted solutions, and one at $\theta=0$. (b) Solutions r_1 and r_2 of the zero-force equation are determined by the intercepts of W/h^2 with $\sigma(r)/r$. If $W/h^2 > \max(\sigma/r)$ the solutions do not exist. If r_1 or r_2 is greater than h, that solution is unphysical.

and approaches infinity as $\bar{\theta}\to\pm\pi/2$ ($\bar{r}\to 0$). The uniform solutions are determined by the extrema of $f(\bar{\theta})$. Local minima are stable with respect to small changes in $\bar{\theta}$, and local maxima are unstable.

Letting $\sigma(r)=U'(r)$ [Fig. 4(b)], the net force on each molecule is zero when

$$\bar{\sigma}h\sin\bar{\theta}=W\cos\bar{\theta}\sin\bar{\theta}\ , \tag{5}$$

where $\bar{\sigma}=\sigma(\bar{r})$. This has solutions of the form

$$\bar{\sigma}/\bar{r}=W/h^2 \tag{6a}$$

and

$$\bar{r}=h\ . \tag{6b}$$

As illustrated in Fig. 5(b), we may determine solutions r_1 and r_2 ($r_1\le r_2$) of (6a) graphically as the intercepts of the horizontal line W/h^2 with the curve σ/r. Note that r_1 has tilt angle θ_1 and corresponds to a local minimum in $f(\bar{\theta})$, while r_2, with tilt angle θ_2, is a local maximum and is thus unstable. The solution with $\bar{r}=h$ corresponds to an extremum of $f(\bar{\theta})$ at $\bar{\theta}=0$. For certain ranges of the parameters $\bar{\theta}=0$ is a local minimum, and there are three locally stable uniform solutions, at $\bar{\theta}=0$ and $\pm\theta_1$.

The transition between the tilted and untilted phases occurs when $f(\bar{\theta})$ goes from having a single global minimum at $\bar{\theta}=0$ to having a pair of global minima at $\pm\theta_1$, that is, when $r_1=h$. The corresponding curve is illustrated in the phase diagram (Fig. 6), which shows our determination of the minimum-energy configuration for a given chain length g, as a function of the ratio of head-chain to chain-chain coupling strengths W/G, and the size mismatch h/r_0. The transition from the tilted to the untilted phase is second order, because θ_1 approaches zero at the phase boundary. In the tilted phase θ_1 decreases as the coupling strength ratio W/G is increased, and increases as the head-chain mismatch h/r_0 is increased.

When we include the preferred tilt angle $\phi_0\neq 0$ in our model, the transitions become first order, as observed experimentally. However, chain melting is the reason that the transition is first order, rather than the asymmetry of the molecule.

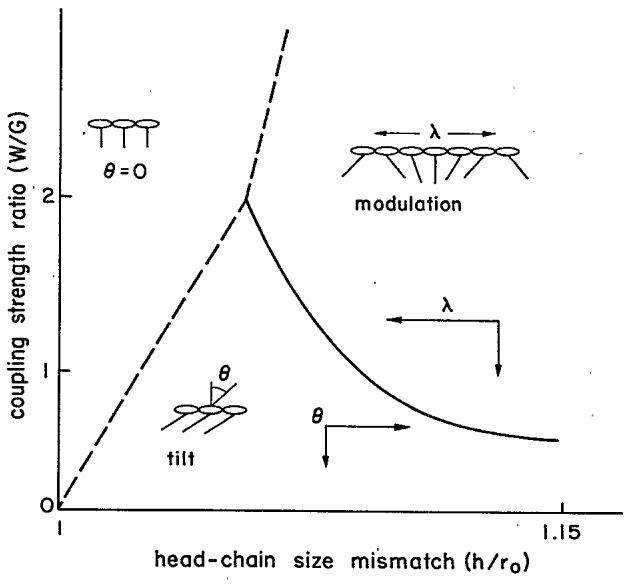

FIG. 6. Theoretical phase diagram for the discrete model, plotted as function of the head-chain to chain-chain coupling strength ratio (W/G), and the size mismatch (h/r_0) for fixed chain length $g/r_0=3$. Solid lines indicate first-order transitions, and dotted lines indicate second-order transitions. The arrows indicate directions in which θ increases in the tilted phase, and λ increases in the modulated phase.

B. Modulation

For any given set of parameter values the minimum-energy configuration can, in principle, be determined using Eq. (3) and the finite difference equation which results from the fact that there can be no net force on any individual molecule. The zero-force equation takes the rather complicated form

$$0=-W\sin\theta_n\cos\theta_n+\sigma(r_n)\left[\frac{h}{2}\sin\left[\frac{\theta_{n+1}+\theta_n}{2}\right]-\frac{g}{2}\cos\left[\frac{\theta_{n+1}-\theta_n}{2}\right]\right]$$
$$+\sigma(r_{n-1})\left[\frac{h}{2}\sin\left[\frac{\theta_n+\theta_{n-1}}{2}\right]+\frac{g}{2}\cos\left[\frac{\theta_n-\theta_{n-1}}{2}\right]\right]\ . \tag{7}$$

When θ_n is a nonconstant function of n, finding solutions becomes a difficult problem. In particular, for a pair of boundary conditions, θ_{n-1} and θ_n, there can be as many as three choices for θ_{n+1} which are consistent with the zero-force equation, two corresponding to local minima, and one corresponding to a local maximum of the three-particle free energy (with periodic boundary conditions). If we only had three particles to worry about it would be a straightforward problem to minimize the free energy; however, as the number of particles, N, becomes large, the number of configurations consistent with the zero-force equation grows exponentially with N.

The free energy is translationally invariant [Eq. (3) does not depend explicitly on n], so in the thermodynamic limit the nonuniform solution is periodic. (For integer wavelengths the solution is exactly periodic, while for noninteger wavelengths the set of θ_n's will not be exactly repeated on subsequent periods, but instead will fall on the same smooth curve.) In order to proceed we must make certain assumptions about the symmetry of the solution. First, we assume that the solution has reflection symmetry, which is a symmetry of the model, that is, invariance with respect to the transformation $\theta\to-\theta$ and $n\to-n$. Second, we assume that the average tilt of the molecules in the modulated phase is zero (this, combined with the first assumption, is equivalent

to assuming that θ passes through zero). Modulation about some nonzero tilt angle will not take maximum advantage of the softness of the chain-chain interaction potential $U(r)$.

Given these constraints, we found that in the modulated phase the minimum-energy configuration has the form illustrated in Fig. 7(a). It is composed of pinched regions of length λ in which the hydrocarbon chains splay inward so that their separation r is nearly r_0. These bulk regions are separated by gaps in the chain spacing. The chain separation at the gap, r_{gap}, is relatively large, taking advantage of the soft part of $U(r)$.

For our calculations we use a Lennard-Jones potential of strength G,

$$U(r)=G\left[\left[\frac{r_0}{r}\right]^{12}-2\left[\frac{r_0}{r}\right]^{6}\right], \tag{8}$$

to represent the interaction between adjacent chains. This choice was made arbitrarily, and the qualitative results are relatively insensitive to the exact form of the potential.[17] The important feature of the potential is that it is soft. As mentioned previously, the strength of the chain-chain interaction is proportional to the chain length ($G \propto g$).

We determine the solutions numerically by choosing the initial pair of boundary conditions $\theta_0=\theta_{\text{gap}}$ and $\theta_1=-\theta_{\text{gap}}$, corresponding to each side of a gap in the chain configuration. To determine θ_2 numerically, we find the roots of the zero-force equation, and select the solution which corresponds to minimum chain separation r_1 between the $n=2$ chain and its predecessor. We proceed in a similar fashion, using θ_1 and θ_2 to determine θ_3, etc., until θ_n changes sign, which is a signal that we have just passed the halfway point of one period of the modulation. Symmetry about $\theta=0$ and periodicity allows us to calculate the free-energy density in the thermodynamic limit using only a finite number of θ_i's. Finally, we minimize the energy with respect to the boundary condition θ_{gap}, which is equivalent to minimization with respect to the number of molecules per period, since each θ_{gap} corresponds to a unique value of λ. (Only one minimization is necessary; we do not have to minimize with respect to θ_1, because we started at a symmetry point in our solution.)

Figure 7(b) shows our numerical results when the modulation wavelength is 20 molecules. As in the $P_{\beta'}$ phase, the density varies periodically. The high-density pinched regions with $r<h$ are energetically favorable. However, the average interchain spacing must be equal to h, so the high-density regions must be separated by gaps, or *defects,* with $r>h$, which are energetically unfavorable. Clearly the predicted modulation is nonsinusoidal. Unlike the $P_{\beta'}$ phase, the modulated phase is symmetric. When a preferred chain tilt angle $\phi_0\neq 0$ is included in our calculations, breaking the symmetry of the model, the modulated phase becomes asymmetric.

Figure 6 illustrates the region of the phase diagram where the modulated solution has lower energy than either the tilted or untilted uniform solution. In Fig. 8 we plot our numerical results for the variation of the wavelength in the modulated phase as we approach each of the phase boundaries. The transition between the $\theta=0$ phase and the modulated phase appears to be second order: The modulation wavelength λ diverges at the phase

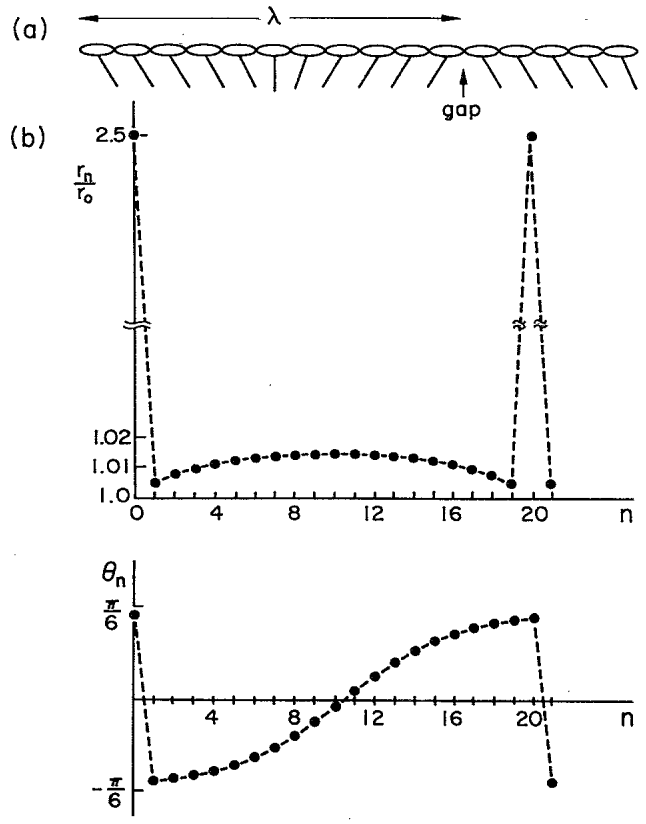

FIG. 7. The minimum-energy configuration in the modulated regime when the wavelength is 20 molecules. (a) The hydrocarbon chain configuration. (b) Numerical results.

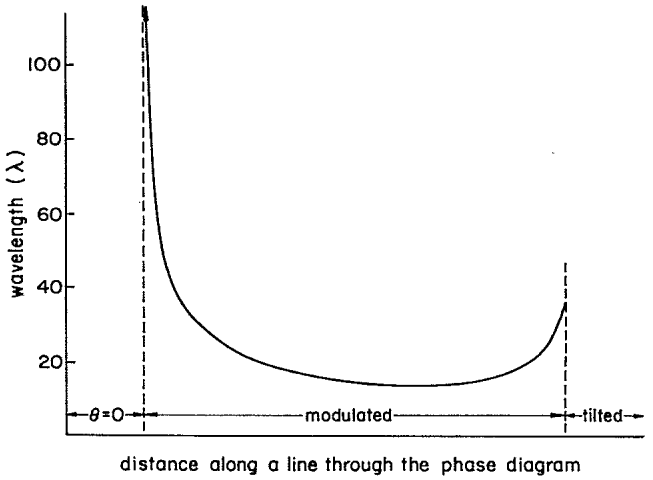

FIG. 8. The variation of the wavelength λ in the modulated phase of the discrete model along a line in the phase diagram which intersects the phase boundaries with both the $\theta=0$ and tilted phases. In the uniform phases λ is trivially infinite. The wavelength appears to diverge approaching the transition to the $\theta=0$ phase, indicating a second-order transition, while approaching the transition to the tilted phase λ increases somewhat, but remains finite, indicative of a first-order transition.

boundary and θ_n approaches zero for almost all n, except for a few of the chains on each side of the gaps. The transition between the tilted uniform phase and the modulated phase appears to be first order: As we cross the phase boundary the solution goes discontinuously from a constant nonzero tilt to nonzero, finite-wavelength modulation about $\theta=0$. Furthermore, in the region of the phase diagram where the tilted phase is the global minimum of the free energy, a modulated solution exists and is a local minimum with somewhat higher energy than the tilted solution, while in the region where the $\theta=0$ phase is the global minimum of the free energy, no finite-wavelength local minimum of the free energy exists.

We studied the variation of λ with the various parameters in our theory. Numerically we found that near the phase boundary with the tilted phase when the wavelength is relatively large (roughly 10 or more molecules per period) the dependence of λ on the chain length is strikingly linear. This result is in good agreement with the experimental results of Wack and Webb.[5] Using x-ray diffraction they measured the ripple wavelength as a function of hydration for chain lengths ranging between 12 and 19 carbons. When the data is rescaled according to a linear dependence of wavelength on the number of carbons, the curves collapse onto a single curve of λ versus hydration. In our model, the increase of λ with chain length follows intuitively because the chains can splay inward less and still maintain the same average separation. In addition, λ decreases as the head-chain mismatch is increased, because the chains must tilt more to maintain the same average separation. Finally, λ decreases as the coupling strength ratio W/G is increased, because strain builds up more quickly moving away from the center of the pinched region.

The variation of λ with the parameters in our theory can also be deduced from a "back-of-the-envelope" calculation, for the free energy in the modulated phase. In the pinched region the characteristic change in tilt for a pair of neighboring molecules is

$$\Delta\theta=\theta_{n+1}-\theta_n=(h-r_0)/g \ . \tag{9}$$

This is the change in tilt necessary when a pair of chains with opposite tilt, $\theta_n=-\theta_{n+1}$, have $r_n=r_0$. If we set the zero of energy at the bottom of the chain-chain interaction potential, them if all of the chains are separated by roughly r_0, the main contribution to the free-energy density from the bulk region comes from strain of the head-chain interaction. Thus

$$f_{\text{bulk}}\approx\frac{1}{\lambda}\int_{-\lambda/2}^{\lambda/2}\tfrac{1}{2}W(n\,\Delta\theta)^2dn=\tfrac{1}{12}W(\Delta\theta)^2\lambda^2 \ . \tag{10}$$

Furthermore, if r_{gap} is large, the contribution to the free-energy density which comes from the gap is given roughly by the depth of the chain-chain interaction potential,

$$f_{\text{gap}}\approx\frac{G}{\lambda} \ . \tag{11}$$

Hence the total free-energy density is

$$f=f_{\text{bulk}}+f_{\text{gap}}\approx\tfrac{1}{12}W(\Delta\theta)^2\lambda^2+\frac{G}{\lambda} \ . \tag{12}$$

This must be minimized with respect to λ, in which case we find

$$\lambda=\left[\frac{6G}{W(\Delta\theta)^2}\right]^{1/3}=\left[\frac{6Gg^2}{W(h-r_0)^2}\right]^{1/3} \ . \tag{13}$$

This gives rise to the same variation of λ with the parameters that was discussed above. Because $G\propto g$ the wavelength is linearly proportional to the chain length. In addition, this formula gives an estimate of λ in the modulated phase. Typical molecular dimensions suggest that h/r_0 is approximately 1.1 to 1.2, and g/r_0 is roughly 2.5 to 3.5. In the modulated phase we find numerically that a typical value is $W/G\approx1$. This leads to values of λ ranging between 10 and 20 molecules per period, which is consistent with our numerical results, and which is in good agreement with experiment. We summarize our results in our comparison of the theoretical and experimental phase diagrams.

IV. COMPARISON OF THEORETICAL AND EXPERIMENTAL PHASE DIAGRAMS

Because the principal degrees of freedom (temperature and concentration) which drive the transition do not appear explicitly in our model, we cannot make direct comparisons between the phase diagram predicted by our model and the experimental phase diagram. Nonetheless, it is useful to compare the trends predicted by our theory to the properties of the experimental system. There are three relevant parameters in our theory which determine the form of the minimum-energy configuration: (1) the size mismatch between head groups and chains, h/r_0, (2) the ratio of head-chain to chain-chain interaction strengths, W/G, and (3) the chain length g which can be scaled by another appropriate length in the problem, say r_0.

In the theroetical phase diagram (Fig. 6), we plot the minimum-energy configuration as a function of the coupling strength ratio, W/G, and the size mismatch, h/r_0 for a fixed value of g. The theory predicts that the transition between the tilted and modulated phases is first order, while the other transitions are second order. The arrows indicate directions of increasing tilt in the uniform tilted phase, and increasing λ in the modulating phase.

We compare these results with a typical experimental phase diagram, illustrated in Fig. 9, which is plotted as a function of temperature and hydration. Experimentally, both the pretransition and the main transition are first order, and both transition temperatures increase as the hydrocarbon chain length is increased. As in the theoretical phase diagram, in Fig. 9 the arrows indicate directions of increasing tilt in the $L_{\beta'}$ phase, and increasing λ in the $P_{\beta'}$ phase. In the $L_{\beta'}$ phase, the tilt angle ϕ increases as the hydration is increased, and decreases as the temperature is increased.[6,18] In the $P_{\beta'}$ phase, the ripple wavelength increases approximately linearly as the hydrocarbon chain length increases, and decreases as the

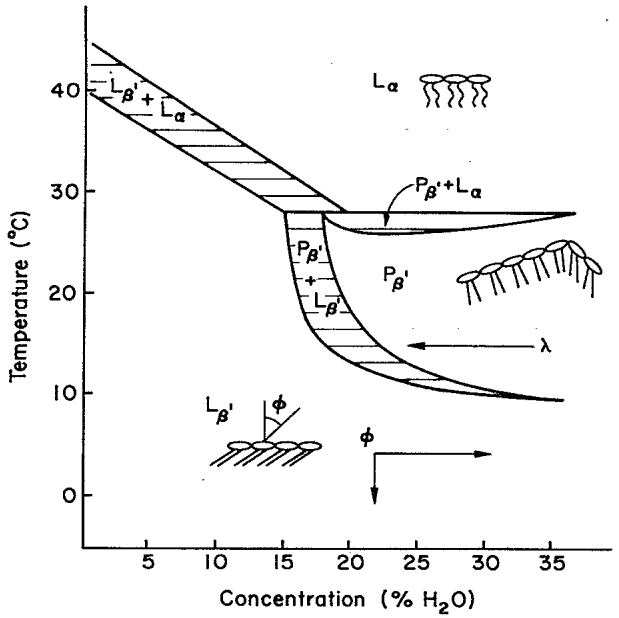

FIG. 9. Experimental phase diagram for DMPC, plotted as a function of temperature and hydration. As in the theoretical phase diagram (Fig. 6), the solid lines indicate first-order transitions, and the arrows indicate directions of increasing tilt in the $L_{\beta'}$ phase, and increasing λ in the $P_{\beta'}$ phase. The phase diagram is based on the results of Janiak, Small, and Shipley (Ref. 18).

hydration is increased,[5] but is relatively insensitive to changes in temperature.

In both theory and experiment the increase in the modulation wavelength is strikingly linear as the hydrocarbon chain length is increased, and the modulation period is typically in the range of 10–20 molecules. In both cases the transition between tilted and modulated phases is first order; however, experimentally the most important feature making the transition first order may be the melting of a few of the hydrocarbon chains.

In our theory both transitions to the $\theta=0$ phase are second order, while experimentally they are first order. This is clearly a weakness of the theory. However, because chain melting is the driving force behind the main transition, and we have not explicitly included melting in our model, it is not surprising that some aspects of the transition to L_α are not well described by our theory. The coarse-grained free energy [Eq. (3)] which we propose is based on what we believe are the most important microscopic features responsible for the $L_{\beta'} \rightarrow P_{\beta'}$ transition. An extension of this model which includes melting should provide a more accurate description of the main transition.

In addition, experimentally both the pretransition and the main transition temperatures increase and approach one another as the hydrocarbon chain length is increased. While temperature does not appear explicitly in our model, some of the parameters (e.g., the ratio of the interaction strengths) may depend implicitly on temperature. Nonetheless, this effect does not show up in our model. In fact, when the g dependence of the coupling strength ratio is scaled out in our plot of the phase diagram [W/G is replaced by $W/(G/g)$ in Fig. 6], so that the vertical axis might scale as some function of the temperature independent of g, then the position of the phase boundary between the tilted and modulated phases is quite insensitive to g. Again, we believe that a more careful treatment of the chains, including melting, is necessary to see this effect.

While we do not attempt to match the parameters in our theory to the experimental parameters, we note that there are some basic trends in the two phase diagrams which agree. In each phase diagram there is an axis along which the angle in the tilted phase increases (h/r_0 and hydration) and an axis along which it decreases (W/G and temperature). Along the axis for which the tilt angle increases, λ decreases in both theory and experiment.

In our theory, the modulated phase is symmetric and flat while experimentally the layers bend out of the mean bilayer plane forming an asymmetric sawtooth pattern. As previously stated, in order to break the symmetry of the modulation, we must break the symmetry of the model, by, for example, including the preferred tilt angle $\phi_0 \neq 0$. In order to see rippling out of plane in the context of our model, the rigidity of the layers must be relaxed (the rigidity of the layers will, for example, depend on the interlayer interactions). If this is treated as a small perturbation, and the energy of the other half of the bilayer is also accounted for, then the layers should bend at the gaps, forming a sawtooth pattern. Figure 2 illustrates how we believe these effects as well as melting should alter the modulated phase predicted by our model.

V. CONTINUUM LIMIT WITH DEFECTS

In this section we look at the long-wavelength limit of the free-energy density [Eq. (3)]. We recall that in the modulated phase, the minimum-energy configuration is composed of periodic sequences of spontaneous inward splay of the hydrocarbon chains, separated by gaps. In the long-wavelength limit, the discrete functions θ_n (which describes the tilt of the chains with respect to the head group layer) and r_n (which describes the chain separation) approach continuous functions except at the gaps, where they are discontinuous. For this reason, special attention must be paid to the term which accounts for the energy of the gaps.

For convenience, in this section we will redefine the chain separation

$$r_n = h - \frac{h}{2}\left[\frac{\theta_{n+1}+\theta_n}{2}\right]^2 - g\frac{(\theta_{n+1}-\theta_n)}{2}, \tag{14}$$

and the harmonic head-chain interaction will be replaced by

$$E_n = \tfrac{1}{2}W\theta^2 . \tag{15}$$

We emphasize that formally we are *not* making a small-angle approximation; instead we redefine these quantities in a manner that will be convenient for our later use.

We could just have easily used these forms for r and the head-chain interaction in our earlier analysis and obtained qualitatively similar results.

Next we rewrite Eq. (3) so that the reflection symmetry of the model holds explicitly for each term in the sum:

$$f=\frac{1}{N}\sum_{n=1}^{N}\frac{U(r_n)+U(r_{n-1})}{2}+\tfrac{1}{2}W\theta_n^2 \ . \tag{16}$$

Because the solution is periodic, the average over N particles can be replaced by an average over one period λ. We let $n=0$ correspond to the center of the bulk region. From our numerical results we know that throughout the continuous region $\Delta r_n=r_n-r_0$ is small. Therefore, in this region the soft part of the chain-chain interaction is not important, and we may replace $U(r)$ with a parabola centered at r_0. Thus

$$f=\frac{1}{\lambda}\sum_{n=-\lambda/2}^{\lambda/2}\left[U(r_0)+\frac{\sigma'(r_0)}{2}\left[\frac{(\Delta r_n)^2+(\Delta r_{n-1})^2}{2}\right]+\tfrac{1}{2}W\theta_n^2\right]+f_{\text{defect}} \ , \tag{17}$$

where f_{defect} is the energy associated with introducing a gap in the continuous solution.

In order to calculate the energy of the defect we note that if $\theta(\lambda/2)\equiv\theta_{\text{gap}}$ is the tilt angle just before a gap, and $\theta(-\lambda/2)\equiv-\theta_{\text{gap}}$ (by the $\theta\rightarrow-\theta$ symmetry of the solution) is the tilt right after a gap, then the chain spacing at the gap is given by

$$r_{\text{gap}}=h+g\theta_{\text{gap}} \ . \tag{18}$$

Therefore the energy of the defect averaged over one modulation period is

$$f_{\text{defect}}=\frac{1}{\lambda}\left[U(r_{\text{gap}})-U(r_0)-\frac{\sigma'(r_0)}{2}(\Delta r_{\lambda/2})^2\right] \ . \tag{19}$$

The last two terms in the above expression are the energy that the last chain before the gap would have had if no defect were present, and must be substracted from the interaction energy of the chains on either side of the gap. While the nonlinearity of the chain interaction potential is not important for the continuous part of the configuration, it is a crucial feature of the defect energy.

Now we are ready to formally take the continuum limit, in which $\theta_{n+1}-\theta_n$ is replaced by a Taylor expansion of a slowly varying continuous function $\theta(x)$ which coincides with θ_n for integer values of x. Letting $\theta'=d\theta/dx$, to second order in gradients $r(x)$ is given by

$$r(x)=h-\frac{h}{2}\left[\theta+\frac{\theta'}{2}+\frac{\theta''}{4}\right]^2-g\left[\frac{\theta'}{2}+\frac{\theta''}{4}\right] \ . \tag{20}$$

Next we substitute this in the free energy (17), again keeping terms to second order in gradients. After integrating the second derivative term by parts (the surface term is odd, and consequently does not contribute), the free-energy density is given by

$$f=\frac{1}{\lambda}\int_{-\lambda/2}^{\lambda/2}dn\,(U(r_0)+\tfrac{1}{2}\sigma'(r_0)\{[h(1-\theta^2/2)-r_0]^2-g[h(1-\theta^2/2)-r_0]\theta'+\tfrac{1}{4}[g^2+h(h-r_0)-\tfrac{3}{8}h^2\theta^2](\theta')^2\}+\tfrac{1}{2}W\theta^2)+f_{\text{defect}} \ . \tag{21}$$

It is important to note that we cannot ignore the term proportional to θ', which is a total divergence term. This term can be integrated exactly, producing a term which is evaluated on the surface (end points of integration). In many systems only the bulk terms contribute to the free-energy density in the thermodynamic limit, and surface terms can be ignored. However, because the gaps correspond to non-negligible internal surface area this term makes a nonzero contribution to the total free-energy density.

The last term in the defect energy may also be expanded to second order in gradients of θ at the boundary. The result is an expression similar to the one that multiplies $\sigma'(r_0)/2$ in the integral, except it is evaluated at $x=\lambda/2$. In this expansion clearly $\theta'(\lambda/2)$ is the gradient of the continuum solution extended to $x=\lambda/2$, and not the δ function associated with the gap.

The free energy (21) is stable with respect to the addition of small gaps. When θ_{gap} is small the leading contribution from the integral is the linear total divergence term, which when integrated becomes

$$\frac{-\sigma'(r_0)g(h-r_0)\theta_{\text{gap}}}{\lambda} \ .$$

However, this is exactly canceled by the linear contribution in the expansion of the defect core energy $U(r_{\text{gap}})$. Furthermore, we find that the quadratic contribution is always positive. Hence the insertion of infinitesimal gaps does not lower the energy, and it is safe to assume the gaps are not small.

While Eq. (21) most accurately describes the continuum limit of the free energy associated with the discrete model, it is more useful to analyze a simpler expression which retains the most important physical features of the system, and has the added advantage that we can obtain analytical results. First, we ignore the θ dependence of the coefficients of the gradient terms. While these terms are in no sense infinitesimal, in each case they are substantially smaller then the gradient terms with constant coefficients [for example, in the coefficient of $(\theta')^2$ the dominant term is g^2, since $g/r_0\sim3$, while $h/r_0\sim1.2$ so that the additional terms nearly cancel]. Second, be-

cause the gaps are large we set the defect energy equal to a constant $f_{\text{defect}}=F/\lambda$, which corresponds roughly to the well depth of the chain-chain interaction potential. After suitable rescaling of f, θ, and x, the free-energy density becomes

$$f=\frac{1}{\lambda}\int_{-\lambda/2}^{\lambda/2}[\tfrac{1}{2}m\theta^2+\tfrac{1}{4}\theta^4+\tfrac{1}{2}(\theta'-\theta_0')^2]dx+1/\lambda\ . \quad (22)$$

The first two terms in the integrand will be minimized when $\theta=0$ for $m>0$, or when $\theta=\pm\sqrt{|m|}$ for $m<0$, corresponding to $\theta=0$ and the tilted solutions, respectively. The gradient term is minimized when $\theta'=\theta_0'$, a positive constant. The local low-energy configuration is illustrated in Fig. 10. The first two chains splay inward towards one another, so that the change in angle is $\Delta\theta\approx\theta_0'$. However, as one moves along the head group axis away from this point, maintaining a positive gradient in θ, strain builds up as θ gets large. (In addition, much later one runs into the topological constraint, that $\theta<\pi/2$: i.e., the chains cannot pass through the head group layer.) Because the local low-energy configuration cannot be satisfied everywhere, we say the system is *frustrated.* However, gaps can act to relieve the strain. Rescaling has allowed us to set the core energy of the defect equal to a constant, so for convenience in Eq. (22) we have set this energy equal to one. Therefore this simple theory has only two parameters, m and θ_0', which will be the axes for the phase diagram for this model.

The frustration is associated with the total divergence term, $-\theta_0'\theta'$, which is the cross term of the gradient term in the free energy, and it may be thought of in two ways. First, as previously stated, it produces a spontaneous splay in the hydrocarbon chain positions in the bulk. Second, when integrated this term becomes the surface term $-2\theta_0'\theta_{\text{gap}}$, which makes a negative contribution to the free-energy density at the defects. Viewing the frustration the second way, we find that the modulated phase is preferred when the net energy cost of introducing a defect becomes sufficiently negative.

We now proceed with the analysis of the free energy (22). In the bulk, the Euler-Lagrange equations tell us

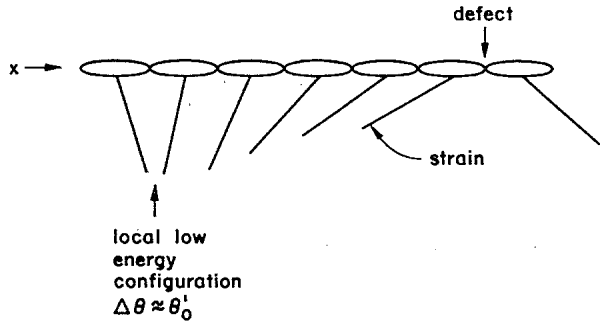

FIG. 10. The molecules on the left are in the local low-energy configuration. However, if we move to the right of these molecules while maintaining a positive gradient in θ, strain builds up as θ becomes large. Gaps can act to relieve this strain.

that θ satisfies the second-order differential equation

$$\theta''=m\theta+\theta^3\ . \quad (23)$$

When $m>0$ this has an exact solution of the form

$$\theta(x)=\sqrt{m}\ \tan(\sqrt{m}/2x)\ , \quad (24)$$

while when $m<0$ an exact solution is

$$\theta(x)=\sqrt{|m|}\ \tanh(\sqrt{|m|}/2x)\ . \quad (25)$$

However, for given values of the parameters m and θ_0', these will not in general be the minimum-energy solutions. We would like to be able to construct an explicit analytical solution to (23) in terms of an arbitrary pair of boundary conditions, and then minimize with respect to the boundary conditions. However, because (23) is nonlinear this cannot be easily done. Instead we use the following trick, which allows us to convert the bulk contribution to f [i.e., the integral in (22)] to a total divergence.

By analogy with Lagrangian mechanics, because the integrand in Eq. (22) does not depend explicitly on x, the timelike variable, there is a formal energy E, which is conserved (i.e., it has the same value for all x),

$$E=\tfrac{1}{2}[(\theta')^2-(\theta_0')^2]-\tfrac{1}{2}m\theta^2-\tfrac{1}{4}\theta^4\ . \quad (26)$$

E is not the free-energy density, which in the modulated phase is clearly a nonconstant function of x. It turns out that $-E$ is the free-energy density in the uniform phases.

We can rewrite the free-energy density in terms of the constant E,

$$f=\frac{1}{\lambda}\int_{-\lambda/2}^{\lambda/2}(\theta')^2dx-\frac{2\theta_0'\theta_{\text{gap}}}{\lambda}-E+\frac{1}{\lambda}\ . \quad (27)$$

Using E again, we solve for θ' in terms of E and θ, to convert the integral over x to an integral over θ

$$f=\frac{1}{\lambda}\int_{-\theta_{\text{gap}}}^{\theta_{\text{gap}}}(2E+(\theta_0')^2+m\theta^2+\tfrac{1}{2}\theta^4)^{1/2}d\theta-\frac{2\theta_0'\theta_{\text{gap}}}{\lambda}-E+\frac{1}{\lambda}\ , \quad (28)$$

where

$$\lambda=\int_{-\theta_{\text{gap}}}^{\theta_{\text{gap}}}\frac{d\theta}{(2E+(\theta_0')^2+m\theta^2+\tfrac{1}{2}\theta^4)^{1/2}}\ . \quad (29)$$

What remains is to minimize the free-energy density with respect to two boundary conditions.

For convenience, we choose these boundary conditions to be the tilt angle at the gap, θ_{gap}, and the derivative of θ at zero, $\theta'(0)$. Now E has the same value for all x, and at $x=0$, it takes the simple form

$$E=\tfrac{1}{2}\{[\theta'(0)]^2-(\theta_0')^2\}\ . \quad (30)$$

Consequently our minimization with respect to θ_{gap} and $\theta'(0)$ can equally well be thought of as a minimization with respect to θ_{gap} and E.

We studied this model numerically, and found that all of the phase transitions are second order: In the modulated phase the wavelength λ diverges as we approach

the phase boundaries. The minimum-energy configurations near the phase boundaries are shown in Fig. 11. First, as illustrated in Fig. 11(a), near the phase boundary with the $\theta=0$ phase most of the chains have $\theta\approx 0$, and only a few chains near the gaps have a substantially larger tilt angle. In this case, $\theta'(0)$ goes to zero as we approach phase boundary. Second, as illustrated in Fig. 11(b), near the phase boundary with the tilted phase, the minimum-energy configuration approaches a solitonlike structure (in which the antisoliton counterparts are the gaps), where almost half of the chains have $\theta\approx -\sqrt{|m|}$, and the other half have $\theta\approx\sqrt{|m|}$, where $\theta=\pm\sqrt{|m|}$ is the tilted solution. In the second case, the minimum-energy solution approaches (25), and $\theta'(0)$ becomes asymptotically equal to $|m|/\sqrt{2}$. In each case these special values of $\theta'(0)$, and the corresponding values of E, make the integrals in (28) and (29) particularly easy to evaluate, and consequently, we obtain the phase boundaries analytically. We give only the results here. The details can be found in Appendix B.

In the phase diagram (Fig. 12), we plot the critical lines separating different types of order. The vertical axis is the coefficient of the quadratic term in free energy, m, and the horizontal axis is the preferred gradient θ_0'. For sufficiently small values of θ_0' a uniform phase will be preferred, and the transition between the uniform phases $\theta=0$ and the tilted phase occurs along the line

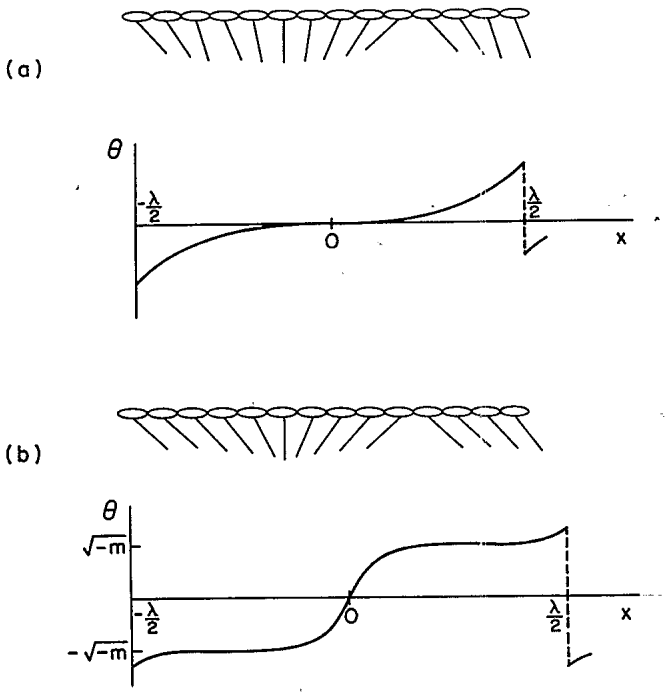

FIG. 11. Minimum-energy configurations in the modulated phase near the phase boundaries in the continuum model. (a) Near the phase boundary with the uniform $\theta=0$ phase most of the chains have $\theta\approx 0$ except for a few of the chains near the gaps. (b) Near the phase boundary with the uniform tilted phase approximately half of the chains have $\theta\approx -\sqrt{|m|}$ and half of the chains have $\theta\approx\sqrt{|m|}$, forming a solitonlike structure in which the antisoliton counterparts are the gaps.

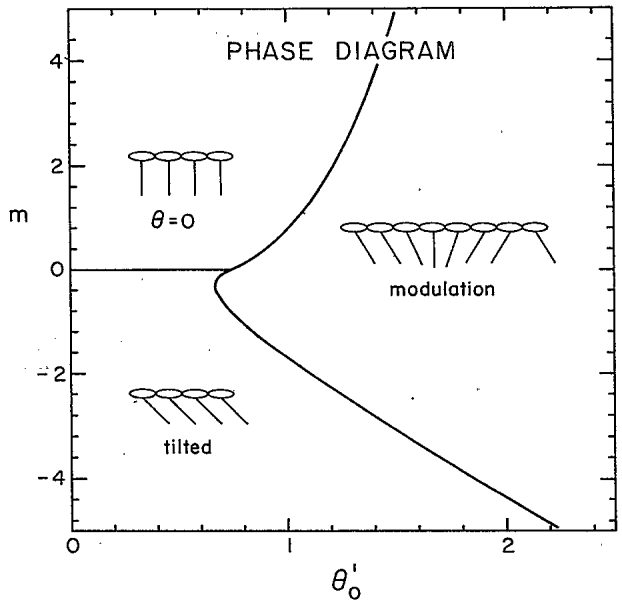

FIG. 12. Phase diagram for the continuum model, plotted as a function of the coefficient of the quadratic term m, and the preferred gradient θ_0' [Eq. (22)]. All transitions are second order, and the results are obtained analytically.

$m=0$. The transition between the $\theta=0$ phase and the modulated phase occurs along a curve which satisfies

$$\tfrac{4}{3}(m+\tfrac{1}{2}\theta_{\rm gap}^2)^{3/2}-\tfrac{4}{3}m^{3/2}-2\theta_0'\theta_{\rm gap}+1=0\ , \tag{31}$$

where

$$\theta_{\rm gap}=\{-m+[m^2+(\theta_0')^2]^{1/2}\}^{1/2}\ . \tag{32}$$

The phase boundary separating the tilted phase from the modulated phase satisfies

$$\sqrt{2}(-|m|\theta_{\rm gap}+\tfrac{1}{3}\theta_{\rm gap}^3+\tfrac{4}{3}|m|^{3/2})-2\theta_0'\theta_{\rm gap}+1=0\ , \tag{33}$$

where

$$\theta_{\rm gap}=(|m|+\sqrt{2}\theta_0')^{1/2}\ . \tag{34}$$

These two curves are illustrated in the phase diagram. They intersect at the point

$$m=0,\quad \theta_0'=\frac{3^{2/3}}{2^{3/2}}\ , \tag{35}$$

where they also meet the boundary between the tilted and $\theta=0$ phases. Hence this is a multicritical point for this model. It is interesting to note that near the multicritical point the tilted phase is reentrant (i.e., for fixed θ_0', as m increases, there is a transition from tilt to modulation, followed by a transition back to tilt before the $\theta=0$ phase is reached). Asymptotically, as m gets large and positive the critical curve between the $\theta=0$ phase and the modulated phase approaches

$$\theta_0'=\tfrac{3}{5}m^{1/4}\ , \tag{36}$$

whereas, when m becomes large and negative, the phase boundary separating tilt from modulation approaches a

line $\theta_0' \propto m$.

In Fig. 13 we plot the variation of the modulation wavelength for a fixed value of m as we approach the phase boundary. Near the phase boundary our numerical results are in good agreement with the asymptotic analytical results, which are given in Appendix B.

VI. DISCUSSION

We began with a one-dimensional discrete model for the ripple phase based on the packing competition between head groups and chains, and found that in one regime the minimum-energy configuration was periodic, composed of high-density regions in which the chains splay inward, separated by gaps in the chain spacing. We then studied the continuum limit of this model, and found that the most important features were contained in a frustrated ϕ^4 theory with a defect term. Like the discrete model, the continuum model gave rise to three phases, $\theta=0$, tilted, and modulated. If we make a simple association between the constant coefficients of the gradient terms in the continuum limit (21) of the discrete free energy and the parameters in the ϕ^4 free energy (22), we may obtain a phase diagram for the ϕ^4 theory in terms of the old parameters. We find that it is in rough agreement with phase diagram for the discrete model (Fig. 6). (Recall that the θ dependence of the coefficients of the gradient terms has been ignored in the ϕ^4 theory. At a minimum we expect these terms to renormalize some of the constants, so an exact association is not expected.) In both cases the phase transitions to the $\theta=0$ phase were second order.

The most significant discrepancy between our two theories is the fact that the transition between the tilted and modulated phases is first order in the discrete model, but second order in the continuum model. This is the result of terms we ignored when we went from the continuum limit to the simplified ϕ^4 theory. Experimentally, the most important feature making both the main transition and the pretransition first order may be the melting of the hydrocarbon chains. The fact that the pretransition is weakly first order could be a result of the melting of only a few of the hydrocarbon chains near the gaps. The latent heat of the pretransition is only one-tenth that of the main transition,[7] so if the modulation wavelength is 20 molecules, this is consistent with melting of the hydrocarbon chains on each side of the gap.

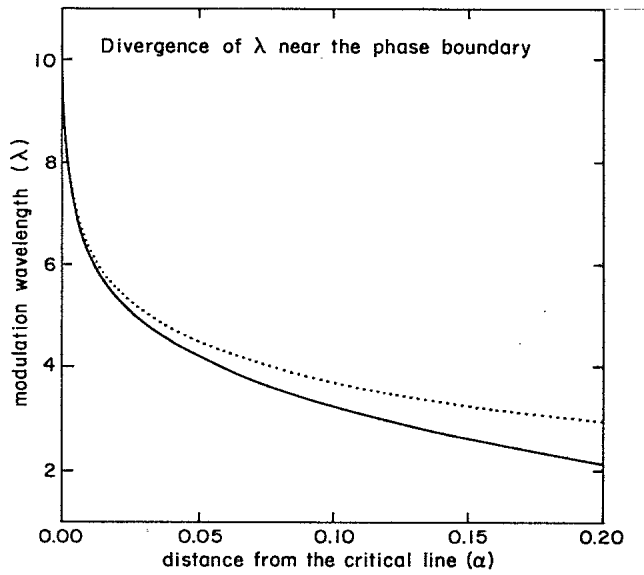

FIG. 13. Variation of the wavelength λ in the continuum model approaching the phase boundary for fixed $m=1$. The dotted line is our numerical results, and the solid line shows our asymptotic analytical results as we approach the phase boundary.

ACKNOWLEDGMENTS

The authors wish to thank D. Wack and M. Schneider for their experimental insights, and S. Leibler, S. Langer, R. Goldstein, and G. Swindle for many useful discussions. This work was supported by National Science Foundation Grant No. DMR-84-51921.

APPENDIX A

In this appendix we give a brief summary of some of the other models which have been proposed for the ripple phase. These fall into three main categories: (1) macroscopic theories, in which the bilayer is treated as a continuous membrane, and its elastic properties are considered; (2) microscopic theories, which are based on properties of individual molecules forming the bilayer; (3) completely different approaches, for example the interactions between adjacent bilayers.

The idea of spontaneous curvature has played a large part in many of the existing macroscopic theories. Tardieu originally suggested an alternate accumulation and release of strain as an explanation for the layer corrugation.[19] In response, Helfrich proposed spontaneous curvature as the specific mechanism which may lower the total elastic energy of a bilayer.[20] Curvature energy is an important consideration in many related phases, like micellar and hexagonal phases. However, in these systems the curvature is much larger.

In many of the microscopic theories the packing hindrance imposed by the head groups is an important feature. Larsson first pointed out the importance of the head-chain packing competition.[21] In his model the ripple phase is represented by a folded lamellar structure which results from alternating tilted and untilted regions. Hawton and Keeler numerically evaluated the van der Waals energy of a spatially modulating layer, and showed that in one regime the free energy is lower than that of a flat layer.[22] Because the pretransition occurs at a temperature near that of the chain melting transition, Falkovitz *et al.*[23,24] have postulated that chain melting is the driving force behind the pretransition as well.

Both Doniach and Falkovitz *et al.* studied continuum theories which are based on the competition between macroscopic curvature energy and microscopic properties of the bilayer. In Doniach's model,[25] as in our work, the local order parameter is the tilt of the chains with respect to the head groups. However, unlike our

model Doniach assumes that the chains are frozen, with constant separation, in a tightly packed crystal structure, and the head group layer is allowed to bend. The pretransition is driven by spontaneous local bilayer curvature, which arises from the electrostatic coupling between water and the head group layer. Doniach begins with a discrete free energy based on two competing interactions (the preferred tilt angle competes with the preferred layer bend). Next he considers the long-wavelength limit, and finds that in one regime periodic modulation in the order parameter lowers the free energy. One of the interesting features of this model, is that like the experimental system, it predicts ripples of two distinct periodicities. However, unlike the experimental system, the modulation is very smooth.

Falkovitz *et al.*[23] and Marder *et al.*[24] stress the importance of the proximity of the melting transition. In their continuum model the ripple phase is composed of alternating regions of fluid and solid chains. Because melting reduces the layer thickness, modulation results in out-of-plane rippling. The free-energy expression they propose is formulated in terms of the local layer thickness. Three terms contribute: a temperature-dependent term favoring either fluid or solid chains, a term proportional to the square of the curvature, and a term which couples the thickness and the curvature. For certain ranges of the coupling strength, they find that between the fluid and solid states, an intermediate modulated phase is favored. As in Doniach's model the modulation in the ripple phase is extremely smooth (in fact, sinusoidal). However, in this model roughly half of the hydrocarbon chains are melted in the modulated phase. This is inconsistent with the fact that experimentally the latent heat of the pretransition is roughly one-tenth that of the main transition, indicating that only a few of the chains are melted in the ripple phase. A better picture would have melted chains only near the peaks and valleys of a sawtoothlike ripple. This sort of configuration may result if chain melting is included in a free-energy expression like the one we propose, which includes defects.

Pearce and Scott[26] studied a model based on the same microscopic mechanisms we base our model on: the competition between the van der Waals attraction between hydrocarbon chains and the packing hindrance imposed by the head groups. In their description, each molecule is treated as a rigid L-shaped object, and interactions between nearest and next-nearest neighbors are taken into account. The Hamiltonian is formulated in terms of the packing configurations of the L's, and in one approximation reduces to the Hamiltonian for the axial nearest-neighbor Ising model (ANNI). This model exhibits a rippled phase between a high-temperature disordered phase and a low-temperature ordered phase.

Other models have also stressed the importance of the size mismatch between head groups and chains. Sackman *et al.* proposed that the ripple structure was the result of a tightly packed chain configuration.[1] Modeling each hydrocarbon chain as a rigid zigzag object, they postulate that adjacent molecules in the bilayer can only shift an integer number of zigzag units with respect to one another, and that this gives rise to an asymmetric rippled structure. However, experimentally it is unlikely that the chains are sufficiently tightly packed for the zigzag shape of the hydrocarbon chains to provide a sufficient packing restriction for this picture to be applicable.

Other models have stressed the importance of interactions between bilayers. Cevc, Zeks, and Podgornik suggested that the pretransition is driven by water-mediated bilayer-bilayer interactions.[27] This may explain why a transition between the $P_{\beta'}$ and $L_{\beta'}$ phases occurs as the concentration is varied at fixed temperature. Goldstein, Leibler, and Lipowsky[28] have shown that at fixed temperature, interlayer interactions can drive the main transition.

Gebhardt *et al.* proposed a model based on the competition between monolayer curvature energy and the compression energy of a bilayer.[29] Chan and Webb suggested that the ripple phase may be the result of a novel type of Martinsitic transformation resulting from molecular-conformation changes.[30]

While in each of these models the proposed microscopic mechanisms responsible for the transition may be different, and lead to different pictures of the ripple phase, the basic philosophy behind most of these calculations is very similar. The authors write down an expression for the free energy of the system in terms of a scalar order parameter (e.g., local chain tilt or layer thickness) which describes the state of the system. This free energy reflects what are believed to be the most important features driving the transition, and should agree with the most general free energy in some appropriate limit. The relative success of each individual theory is measured by how well it agrees with experiment, and depends on how well the model captures the essence of the true driving mechanism.

In principle, one could write down an expression for the free energy in terms of the three-dimensional molecular density which would encompass all of the interactions. Upon integrating over all of the degrees of freedom except for one, one is left with a completely general expression for the course-grained free energy in terms of a single scalar order parameter, which in our model corresponds to θ. A general expression of this form has been derived by Leibler and Andelman[31] for membrane curvature in the low-amplitude limit. Our free energy agrees with the general expression in an appropriate limit, as do the similar free-energy expressions proposed by Doniach, Falkovitz *et al.*, and Marder *et al.* Viewed in this light, the main difference between our model and the others is the fact that our modulated phase has defects (places where the order parameter changes abruptly), while the others do not. In terms of the more general formulation, our model studies the limit in which the length scale for low-density regions shrinks to the size of the lattice spacing.

A model which is very similar to ours was proposed recently by Safran, Robbins, and Garoff[32] to describe surfactants on a surface. Fixing the molecules a constant distance apart from one another, they integrate the chain-chain interaction along the length of each of the

chains and obtain results quite similar to ours. The connection between the two methods is clear. Their integrated interaction may be represented by an effective pair interaction, which is a function of some characteristic chain separation, and the strength of which increases with increased chain length, combined with a harmonic restoring force, which is independent of the chain length, and which arises because the total overlap region decreases when chains are tilted.

APPENDIX B

In this appendix we give details of the analytical calculations of the phase boundaries which separate the modulated phase from the uniform phases, and the divergence of the wavelength as we approach the phase boundaries, in the simplified continuum model. Near the phase boundary with the $\theta=0$ phase, most of the chains have $\theta\approx 0$, except for a few chains near the gaps, as illustrated in Fig. 11(a). Approaching the boundary with the tilted phase, the minimum-energy configuration approaches the solitonlike structure illustrated in Fig. 11(b), and $\theta(x)$ is given approximately by (25). The free-energy density is given by Eq. (28), and the modulation wavelength is given by Eq. (29). Special care must be taken, because λ diverges on the phase boundaries.

As we approach the boundary between the $\theta=0$ phase and the modulated phase, m is positive and the gradient of θ in the center of the bulk region, $\theta'(0)$, becomes small. Consequently the constant E [Eq. (26)] can be written

$$E=-\tfrac{1}{2}(\theta_0')^2+\tfrac{1}{2}\epsilon\ , \tag{B1}$$

where we assume ϵ is small. Substituting this into the free-energy density (28), we find

$$f=\frac{1}{\lambda}\int_{-\theta_{\rm gap}}^{\theta_{\rm gap}}(\epsilon+m\theta^2+\tfrac{1}{2}\theta^4)^{1/2}d\theta-\frac{2\theta_0'\theta_{\rm gap}}{\lambda}$$
$$+\tfrac{1}{2}(\theta_0')^2-\frac{\epsilon}{2}+\frac{1}{\lambda}\ . \tag{B2}$$

When $\epsilon=0$, the integrand has a branch point at $\theta=0$, so we rewrite the integral (which we refer to now as I) as

$$I=2\int_0^{\delta}(\epsilon+m\theta^2+\tfrac{1}{2}\theta^4)^{1/2}d\theta$$
$$+2\int_{\delta}^{\theta_{\rm gap}}(\epsilon+m\theta^2+\tfrac{1}{2}\theta^4)^{1/2}d\theta\ , \tag{B3}$$

where δ is assumed to be small. To leading order only the second integral contributes, so that for $\delta=[m-(m^2-2\epsilon)^{1/2}]^{1/2}=\sqrt{\epsilon/m}+O(\epsilon^{3/2})$,

$$I=\tfrac{4}{3}(m+\tfrac{1}{2}\theta_{\rm gap}^2)^{3/2}-\tfrac{4}{3}m^{3/2}-\frac{\epsilon}{2\sqrt{m}}\ln\epsilon+O(\epsilon)\ . \tag{B4}$$

Similar analysis is necessary to evaluate λ. Again we split the integral into two parts:

$$\lambda=2\int_0^{\delta}d\theta\frac{1}{(\epsilon+m\theta^2+\tfrac{1}{2}\theta^4)^{1/2}}$$
$$+2\int_{\delta}^{\theta_{\rm gap}}d1\frac{\theta}{(\epsilon+m\theta^2+\tfrac{1}{2}\theta^4)^{1/2}}\ . \tag{B5}$$

We find that when ϵ is small and δ has the form specified above, to leading order the first integral is $O(1)$ while the second diverges logarithmically as ϵ approaches zero. Hence we find

$$\lambda=-\frac{1}{\sqrt{m}}\ln\epsilon+O(1)\ . \tag{B6}$$

Therefore, the free-energy density is given asymptotically by

$$f=\tfrac{1}{2}(\theta_0')^2-\frac{\sqrt{m}}{\ln\epsilon}[\tfrac{4}{3}(m+\tfrac{1}{2}\theta_{\rm gap}^2)^{3/2}-\tfrac{4}{3}m^{3/2}-2\theta_0'\theta_{\rm gap}$$
$$+1-A\epsilon][1+O(\ln^{-1}\epsilon)]\ , \tag{B7}$$

where A is a rather complicated constant which depends on m and $\theta_{\rm gap}$. The first term in (B7) is just the energy of the $\theta=0$ solution, so that when $\epsilon=0$, f becomes equal to the energy of the uniform solution. When $\epsilon\neq 0$, f must be minimized with respect to the boundary conditions $\theta_{\rm gap}$ and ϵ. This requires that

$$\frac{\partial f}{\partial\theta_{\rm gap}}=0\ \text{ and }\ \frac{\partial f}{\partial\epsilon}=0\ . \tag{B8}$$

(Positivity of the second derivative verifies that we have indeed located a minimum.) Thus solving self-consistently for small ϵ, the first condition is satisfied when

$$\theta_0'=\theta_{\rm gap}(m+\tfrac{1}{2}\theta_{\rm gap}^2)^{1/2}\ , \tag{B9}$$

while the second is satisfied in the limit $\epsilon\to 0$ only when

$$\tfrac{4}{3}(m+\tfrac{1}{2}\theta_{\rm gap}^2)^{3/2}-\tfrac{4}{3}m^{3/2}-2\theta_0'\theta_{\rm gap}+1=0\ . \tag{B10}$$

The first of these equations can be used to eliminate $\theta_{\rm gap}$ from the second, and the resulting equation determines the phase boundary between the modulating phase and the $\theta=0$ phase.

To determine how λ diverges as we approach the phase boundary we need to consider the corrections to the free energy which are higher order in ϵ. In a previous calculation we obtained the variation of λ with ϵ [Eq. (B6)], which is related to the effective energy E by (B1). However, this tells us nothing about how λ varies as, for example, θ_0' approaches its critical value, $\theta_0'^c$, for a fixed value of m (i.e., approaching the phase boundary from the right-hand side). We define $\alpha=\theta_0'-\theta_0'^c$. Retaining terms to order in $\epsilon/\ln\epsilon$ and $\alpha/\ln\epsilon$ in the free energy [Eq. (B7)], we perform the necessary minimizations [Eq. (B8)], and find that to leading order minimization with respect to $\theta_{\rm gap}$ again results in Eq. (B9). Using this equation we solve for the leading correction in α to $\theta_{\rm gap}$,

$$\theta_{\rm gap}=\theta_{\rm gap}^c+\frac{\theta_0'^c\alpha}{\theta_{\rm gap}^c[(\theta_{\rm gap}^c)^2+m]}\ , \tag{B11}$$

where $\theta_{\rm gap}^c=[-m+(m^2+2\theta_0'^c)^{1/2}]^{1/2}$, is the value of $\theta_{\rm gap}$ along the critical line. Substituting this into the free energy, we find that minimization with respect to ϵ to leading order in ϵ and α yields

$$\frac{A}{\ln\epsilon}+\frac{2\theta_{\rm gap}^{c}\sqrt{m}\,\alpha}{\epsilon\ln^2\epsilon}=0\ . \tag{B12}$$

This is satisfied when

$$\epsilon\ln\epsilon=\kappa\alpha\ , \tag{B13}$$

where κ is a positive constant which depends on m and $(\theta_0')^c$. These equations, combined with Eq. (B6), implicitly determine λ as a function of α

$$\alpha=\kappa\lambda e^{-\sqrt{m}\,\lambda}\ .$$

The results for $m=1$ are illustrated in Fig. 13.

We proceed similarly for the phase boundary between the modulated and tilted phases. In this case, $m<0$ and $\theta'(0)$ approaches $|m|/\sqrt{2}$, so we can write

$$E=\tfrac{1}{4}m^2-\tfrac{1}{2}(\theta_0')^2+\tfrac{1}{2}\epsilon\ , \tag{B14}$$

where again ϵ is presumed small. When E is substituted into the free-energy density, we have

$$f=\frac{1}{\lambda}\int_{-\theta_{\rm gap}}^{\theta_{\rm gap}}[\epsilon+\tfrac{1}{2}(-|m|+\theta^2)^2]^{1/2}d\theta-\frac{2\theta_0'\theta_{\rm gap}}{\lambda}+\tfrac{1}{2}(\theta_0')^2-\frac{m^2}{4}-\frac{\epsilon}{2}+\frac{1}{\lambda}\ . \tag{B15}$$

This time, when $\epsilon=0$, the square root has a branch point at $\theta=\pm\sqrt{|m|}$, the angle of the uniform tilted solution. We find that to leading order the integral (again called I) is given by

$$I=\sqrt{2}(-|m|\theta_{\rm gap}+\theta_{\rm gap}^3/3+\tfrac{4}{3}|m|^{3/2})-\sqrt{2/|m|}\,\epsilon\ln\epsilon+O(\epsilon)\ . \tag{B16}$$

To evaluate the integral for λ

$$\lambda=2\int_0^{\theta_{\rm gap}}\frac{d\theta}{[\epsilon+\tfrac{1}{2}(-|m|+\theta^2)^2]^{1/2}}\ , \tag{B17}$$

we break the interval in to three pieces, $[0,\sqrt{|m|}-\delta/2]$, $[\sqrt{|m|}-\delta/2,\sqrt{|m|}+\delta/2]$, and $[\sqrt{|m|}+\delta/2,\theta_{\rm gap}]$, where $\delta=O(\sqrt{\epsilon})$, and again find that as ϵ approaches zero the wavelength diverges logarithmically

$$\lambda=-\sqrt{2/|m|}\,\ln\epsilon+O(1)\ . \tag{B18}$$

This leads to the following asymptotic form of the free-energy density:

$$f=\tfrac{1}{2}(\theta_0')^2-\frac{m^2}{4}-\frac{\sqrt{|m|}}{\sqrt{2}\,\ln\epsilon}[\sqrt{2}(-|m|\theta_{\rm gap}+\tfrac{1}{3}\theta_{\rm gap}^3+\tfrac{4}{3}|m|^{3/2})-2\theta_0'\theta_{\rm gap}+1+O(\epsilon)][1+O(\ln^{-1}\epsilon)]\ . \tag{B19}$$

Now the first two terms are equal to the energy of the tilted solution, so that f is equal to the free energy of the uniform solution when ϵ approaches zero. As before, when $\epsilon\neq0$ we minimize f with respect to the boundary conditions. This yields the following set of equations (which are self-consistent for ϵ small):

$$\sqrt{2}\theta_0'=-|m|+\theta_{\rm gap}^2\ , \tag{B20}$$

and in the limit $\epsilon\to0$

$$\sqrt{2}(-|m|\theta_{\rm gap}+\tfrac{1}{3}\theta_{\rm gap}^3+\tfrac{4}{3}|m|^{3/2})-2\theta_0'\theta_{\rm gap}+1=0\ , \tag{B21}$$

which determine the phase boundary. Again, retaining corrections to the free energy which are higher order in ϵ allows us to determine the variation of λ in the phase diagram as we approach the phase boundary with the tilted phase.

It is interesting to note that $\theta_{\rm gap}$ does not asymptotically approach the uniform tilted solution $\sqrt{|m|}$ as we approach the phase boundary. Instead, close to the phase boundary, moving out from a central molecule towards the gaps, the minimum-energy configuration has an increasing number of chains with tilt nearly equal to $\sqrt{|m|}$, followed by a few chains with a larger tilt, until the $\theta_{\rm gap}$ which satisfies (B20) is reached. At the phase boundary, the number of chains with tilt near $\sqrt{|m|}$ diverges, and the *gaps* are pushed out to infinity.

[1]See, for example, E. Sackman, D. Ruppel, and C. Gebhardt, in *Liquid Crystals of One and Two Dimensional Order,* edited by W. Helfrich and G. Heppke (Springer-Verlag, New York, 1980), p. 309.

[2]D. Chapman, R. M. Williams, and B. D. Ladbrooke, Chem. Phys. Lipids **1**, 445 (1967).

[3]The same is true for other molecules like phosphatidyl glycerol (PG) which have a tilted $L_{\beta'}$ phase. See, for example, D. Marsh, Biochem. Biophys. Acta **510**, 63 (1978).

[4]J. Zasadzinski and M. Schneider (unpublished).

[5]D. Wack and W. W. Webb (unpublished).

[6]M. J. Janiak, D. M. Small, and G. G. Shipley, Biochem. **15**, 4575 (1976).

[7]J. F. Nagle, Ann. Rev. Phys. Chem. **31**, 157 (1980); J. F. Nagle and D. A. Wilkinson, Biophys. J. **23**, 159 (1978).

[8]P.-G. de Gennes, J. Phys. (Paris) Lett. **44**, L-657 (1983).

[9]C. Godrèche and L. de Seze, J. Phys. (Paris) Lett. **46**, L-39 (1985).

[10]J. P. Sethna, Phys. Rev. B **31**, 6278 (1985).

[11]S. A. Langer and J. P. Sethna, Phys. Rev. A **34**, 5035 (1986).

[12]T. J. McIntosh, Biophys. J. **29**, 237 (1980).

[13]R. J. Wittebort, C. F. Schmidt, and R. J. Griffin, Biochemistry **20**, 4223 (1981); M. Schneider, W. Chan, and W. W. Webb, Biophys. J. **43**, 157 (1983).

[14]See, for example, J. N. Isrealachvili, in *Physics of Amphiphiles: Micelles, Vesicles, and Microemulsions,* edited by. V.

Degiorgio and M. Corti (North-Holland, Amsterdam, 1985), p. 24.

[15]In general, after integrating over all other degrees of freedom, the free energy will be some functional $\mathcal{F}(\ldots,\theta_{n-1},\theta_n,\theta_{n+1},\ldots)$. In the spirit of a gradient expansion in which r represents the first derivative, the free energy can be approximated by some pair interaction $\mathcal{U}(r,\theta)$. For simplicity, we break up $\mathcal{U}(r,\theta)=U(r)+\frac{1}{2}W\sin^2\theta$.

[16]The van der Waals energy of the chains is proportional to the volume of hydrocarbon chains in the bilayer [see, for example, the earlier reference to Nagle (Ref. 7)].

[17]For example, similar results are obtained using the potential for infinitely narrow parallel rigid rods of polarizable media, $U(r)=A/r^{25}-B/r^5$, that was proposed by Salem in L. Salem, J. Chem. Phys. **37**, 2100 (1962).

[18]M. J. Janiak, D. M. Small, and G. G. Shipley, J. Biol. Chem. **254**, 6068 (1979).

[19]A. Tardieu, V. Luzzati, and F. C. Reman, J. Mol. Biol. **75**, 771 (1973).

[20]W. Helfrich, Z. Naturforsch. **29C**, 692 (1974).

[21]K. Larsson, Chem Phys. Lipids **20**, 225 (1977).

[22]M. Hawton and W. J. Keeler, Phys. Rev. A **33**, 3333 (1986).

[23]M. S. Falkovitz, M. Seul, H. L. Frisch, and H. M. McConnell, Proc. Nat. Acad. Sci. U.S.A. **79**, 3918 (1982).

[24]M. Marder, H. L. Frisch, J. S. Langer, and H. M. McConnell, Proc. Nat. Acad. Sci. U.S.A. **81**, 6559 (1984).

[25]S. Doniach, J. Chem. Phys. **70**, 4587 (1979).

[26]P. A. Pearce and H. L. Scott, J. Chem. Phys. **77**, 951 (1982).

[27]G. Cevc, B. Zeks, and R. Podgornik, Chem. Phys. Lett. **84**, 209 (1981).

[28]R. Goldstein, S. Leibler, and R. Lipowsky (unpublished).

[29]C. Gebhardt, H. Gruler, and E. Sackmann, Z. Naturforsch. **32C**, 581 (1977).

[30]W. K. Chan and W. W. Webb, Phys. Rev. Lett. **46**, 39 (1981).

[31]S. Leibler and D. Andelman (unpublished).

[32]S. A. Safran, M. O. Robbins, and S. Garoff, Phys. Rev. A **33**, 2186 (1986).